H.-W. Ou[1]

[1] Lamont-Doherty Earth Observatory, Columbia University, Palisades, NY10964, USA

Corresponding author: Hsien-Wang Ou (hsienou0905@gmail.com)

Key Points:

- Ocean is heated by the annual absorbed solar insolation, which anchors the summer air temperature to control ablation and ice margin
- An eddying ocean has bistates of maximum entropy production, which translate to ice bistates that enable large ice signal via hysteresis
- Hysteresis thresholds are set by the global convective flux lowered during Pleistocene, resulting in transition from 41- to 100-ky cycles

Abstract. The summer air temperature that regulates the ice margin covaries with the sea surface temperature but precedes the ice volume during glacial cycles, suggesting that the ocean is the intermediary of the orbital forcing of the ice sheet. We formulate a minimal model to elucidate the ocean role in the genesis of glacial cycles. We show that, because of the atmospheric coupling, an eddying ocean exhibits bistates of maximum entropy production, which would translate to ice bistates of polar ice cap and Laurentide ice sheet, enabling large ice-volume signal when the bistable interval is crossed by the forcing. Since this bistable interval is set by the global convective flux, it is lowered during Pleistocene cooling, whose interplay with the ice-albedo feedback may account for the mid-Pleistocene transition from 41-ky obliquity cyles to 100-ky ice-age cycles paced by eccentricity. Quantitative tests of the theory and its parsimony in resolving myriad glacial puzzles suggest that the theory has captured the governing physics of the Pleistocene glacial cycles.

Plain Language Summary

Based on observed covarying sea-surface and summer air temperatures through glacial cycles, we posit the ocean as the intermediary of the orbital forcing of the ice sheet. Because of the atmospheric coupling, a turbulent ocean may be bistable, which would translate to that of the ice sheet, enabling large ice-volume signal when the bistable interval is crossed by the orbital forcing. This bistable interval is set by the global convective flux hence is lowered during Pleistocene cooling, resulting in 100-ky ice-age cycles in late Pleistocene paced by eccentricity.

1 Introduction

In late Pleistocene, the global ice volume exhibits pronounced variation at orbital periods (Hays et al. 1976). As Antarctica was iced over about ten million years ago (Berger 1979), the ice-volume signal reflects mainly that of the northern ice sheet, whose correlation with the Milankovitch insolation (MI, all acronyms are listed in Appendix A) supports the astronomical theory that it

is the summer surface-air temperature (SAT) that controls the ice margin (Milankovitch 1941). The orbital forcing of the summer SAT however cannot be direct since the latter is bounded above by the sea-surface temperature (SST) for a convective atmosphere; that is, while there could be short-term or regional departure from this "convective bound", it must generally hold to maintain radiative-convective equilibrium that defines the atmosphere. This convective bound is seen distinctly in the global distribution of the summer SAT and SST in the current climate (Peixoto and Oort 1992, Fig. 10.7, lower panel) and also in their comparable lowering during the last glacial maximum (LGM) revealed in model calculations (Hostetler et al. 1999, Plate 1).

Because of this convective bound, the annual SAT registered in ice cores covaries with the SST through glacial cycles (Dansgaard et al. 1993, Fig. 2d; Labeyrie et al. 1995, Fig. 3), which moreover lead the ice volume by several millennia (Petit et al. 1999; Shackleton 2000). This observation alone suggests that the ocean must be the intermediary of the orbital forcing of the ice sheet, a causal link that is also strongly argued by Broecker and Denton (1989) but often overlooked. It calls into question the widespread practice of linking the summer SAT (or snowline) to MI against an arbitrary reference temperature (Oerlemans 1980; Huybers 2006; Abe-Ouchi et al. 2013) since the only justifiable reference is the varying SST that anchors the summer SAT. As such, a replication of the SST signal should be a prerequisite for proper simulations of the glacial cycles --- a benchmark not yet adequately met.

Since meridional overturning circulation (MOC) is the heat transport mechanism that regulates the SST, the two are expectedly correlated through glacial cycles, with MOC practically shut down during the deep glacial (Broecker and Denton 1989, Fig. 26; Keigwin et al. 1994, Fig. 1; Raymo et al. 1997, Fig. 3; Clark et al. 2006, Fig. 11). Clearly, to capture their observed variability, a mixed-layer ocean model is insufficient (Suarez and Held 1979; Berger et al. 1999), and for primitive-equation models that include the ocean dynamics, the limitation is in their spatial resolution. For coarse-grained ones that do not resolve eddies, MOC takes the form of a laminar cell, which however depends critically on the poorly constrained diapycnal diffusivity (Dalan et al. 2005), so the latter is in effect a free parameter finely tuned to yield the observed state (Rahmstorf et al. 2005). This sensitivity is arguably the artifact of a laminar MOC whereas the observed one is partly composed of random eddies (Auer 1987; Lozier 2010) to be subjected to probability laws of the nonequilibrium thermodynamics (NT). Applying such a law, Ou (2018) deduces that MOC would be propelled toward maximum entropy production (MEP), which is seen later to produce a robust MOC comparable with the observed one. While this tendency in principle is entailed in eddy-resolving calculations, the latter pose a daunting challenge to glacial-cycle simulations because of the long integration needed (see further discussion in Section 5). Our theoretical construct however is free from such restraint, which shows that an eddying ocean contains bistable MEP states to anchor the glacial cycles while resolving some longstanding puzzles.

One such puzzle is the mid-Pleistocene transition (MPT) from 41- to 100-ky cycles when there is no appreciable change in MI (Elkibbi and Rial 2001; Clark et al. 2006). Although early focus was on the genesis of the 100-ky cycles, not to be overlooked is their absence in early Pleistocene, which in fact would weed out some resolutions of the "100-ky problem". These include internal ice-sheet oscillations (Imbrie and Imbrie 1980; Oerlemans 1982; Pollard 1983; Pelletier 2003) and stochastic dynamics (Ghil 1994; Wunsch 2003; Tziperman et al. 2006), as these mechanisms should be operative as well in early Pleistocene when the northern hemisphere glaciation has already set in (Ravelo et al. 2004) and yet there are no 100-ky cycles. Then there are conceptual and dynamical-system models tuned to replicate glacial cycles (Saltzman et al. 1984; Paillard 1998; Imbrie et al. 2011; Crucifix 2013), but since some key parameters do not correspond to measurable quantities hence unconstrained, these models are mostly unfalsifiable to constitute a testable physical theory.

A plausible and well-explored paradigm of the glacial cycles is that the ice sheet is bistable, so eccentricity can generate 100-ky cycles through its modulation of the forcing amplitude, and if the hysteresis thresholds are lowered by the putative decrease of pCO_2 through the Pleistocene, one could have an account of the MPT. But there is little evidence of such pCO_2 trend through the MPT (Honisch et al. 2009) and, given its short equilibration time, pCO_2 variation is more a response than driver of the cooling (Broecker and Denton 1989; Siegenthaler et al. 2005; Ganopolski and Brovkin 2017). Even more seriously, the postulated ice bistability involves an ice-free state (Weertman 1976), which cannot characterize the interglacial, as attested by the present Greenland ice sheet, and if it were realized in early Pleistocene, then the hysteresis paradigm would imply vanishing ice-volume signal, as indeed seen in numerical calculations (Berger et al. 1999; Calov and Ganopolski 2005; Abe-Ouchi et al. 2013) but at considerable odds with observations (Raymo and Nisancioglu 2003). To preserve the hysteresis paradigm therefore, one needs to invoke different bistates, which as we shall see can be engendered by the ocean.

Since the main difference of our theory is an eddying ocean filtering the orbital forcing of the ice margin, we shall formulate a minimal model to isolate this physics. In the following, we elucidate first the inner working of a coupled climate system (Section 2) and then how the orbital forcing is filtered through this system to generate glacial cycles (Section 3). We highlight how the theory may resolve myriad Pleistocene puzzles (Section 4) and provide additional discussion (Section 5) to conclude the paper.

1. Coupled climate model

As a minimal model, we consider a configuration of the North Atlantic as sketched in Fig. 1, for which both ocean and atmosphere are divided into warm and cold masses by mid-latitude fronts and an ice sheet may form on the adjacent continental strip that terminates at the Arctic Ocean. Since both forcing and response of the glacial cycles are dominated by that of the cold boxes, the model variables are the cold-box deviations (primed) from global means (over-

barred), the latter assumed known for simplicity. Retaining dominant balances, the cold-box deficit of the *annual* absorbed shortwave (SW) flux (q') differentiates SST (T'), which then heats SAT (T'_a) by convective and net longwave (LW) fluxes. The accompanying atmospheric heat- hence moisture-transport differentiates the ocean salinity (S') and density (ρ'), the latter drives MOC (K) composed partly of random eddies. For the ice sheet, the total ablation (A_b) and accumulation (A_c) constrain the equilibrium line (EL) altitude (ELA, h_0) hence its x-coordinate (l_0) as well as the ice margin (l).

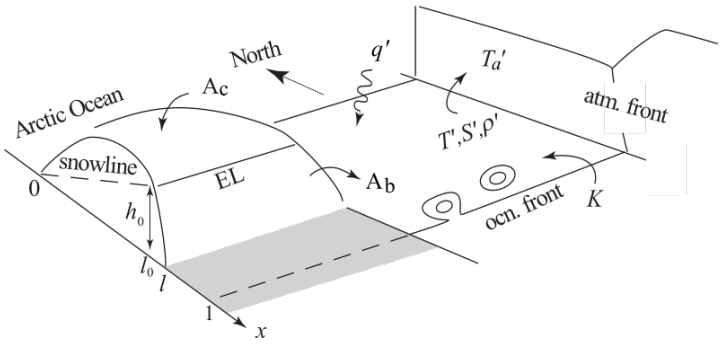

Figure 1: The model configuration of a coupled ocean/atmosphere composed of warm and cold boxes aligned at mid-latitude and an ice sheet on the adjacent continental strip terminating at Arctic Ocean. The model variables include the cold-box deviations from global means of the absorbed SW flux (q'), SST (T'), salinity (S'), density (ρ'), SAT (T'_a), and MOC (K) composed partly of random eddies. The total Ablation (A_b) and accumulation (A_c) constrain the ELA (h_0) hence its x-coordinate (l_0) and ice margin (l).

2.1 Regime diagram

Following Stommel (1961), we illustrate the physics of the climate system via a regime diagram (Fig. 2) whereby cold-box deviations from the global means are plotted against MOC (K). All variables are nondimensionalized, with their scaling definitions and standard values listed in Appendix B. Readers are referred to Ou (2018) for the mathematical derivation, but the following discussion suffices for our purpose. For an infinite K, the ocean is homogeneous, so the SST deficit ($T^{'}$) is zero and the SAT deficit ($T_a^{'}$, referred to the global-mean SST) is lowered by the global convective flux ($\overline{q}_c^{'}$). As K decreases, the subpolar water cools, which however is moderated by the cooling air that reduces the convective flux (the spacing between temperature curves). To balance the LW cooling of the subpolar air, the atmospheric heat transport increases to compensate for the decreasing convective flux. There is however a limit to this atmospheric coupling as the convective flux may not be negative (Section 1), which occurs at (vertical dashed, Ou 2018)

$$T' = 2\overline{q}_c^{'}. \quad (1)$$

Beyond this "convective bound", the atmospheric heat transport has saturated, so the merged temperature would steepen at a faster rate (inverse in K).

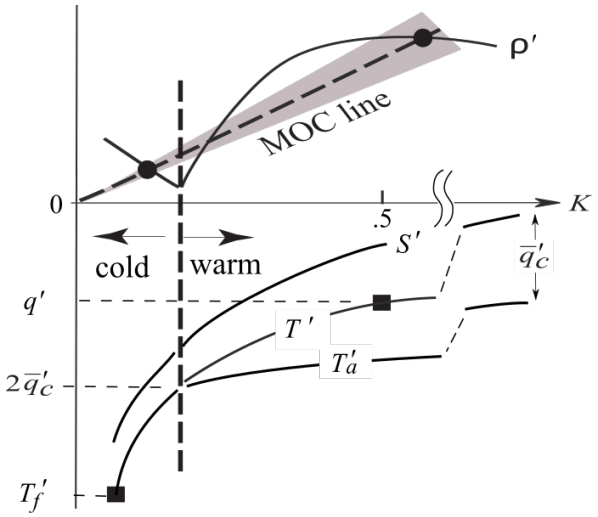

Figure 2: A schematic of the regime diagram in which cold-box deviations (sold lines) from global means are plotted against MOC (K). The vertical dashed line marks the convective bound that divides the warm and cold branches, and the intersect of the MOC line (sloping dashed) with the density curve specifies the climate state (ovals). Subjected to fluctuations (shaded cone), the MOC line would pivot toward MEP states (rectangles), which define the interglacial and glacial states. Marked on the ordinate are forcing ($q^{'}$), global convective flux ($\overline{q}_c^{'}$) and freezing point ($T_f^{'}$).

We next consider the salinity deficit of the subpolar water (S'). Before the convective bound, the decreasing K is compounded by increasing atmospheric heat-hence moisture-transport to sharply freshen the subpolar water; beyond the convective bound, the moisture transport has saturated with the atmospheric heat transport, so the salinity deficit increases as the inverse of K, just like the temperature deficit. The disparate temperature and salinity slopes result in a density surplus ($\rho' = T' - S'$) that has opposite slopes straddling the convective bound, which divides the warm/cold branches.

To determine the climate state from these continua, one needs a constraint on the MOC, which is assumed linear in the density surplus (Stommel 1961; Marotzke and Stone 1995), as indicated in the sloping "MOC line". The proportional constant (inverse of its slope) is referred as "admittance" (drawing its analogy from electrostatics with density/MOC playing the role of voltage/current), and the intersect of the MOC line with the density curve then specifies the climate. In a laminar ocean, the admittance depends on a tuned diapycnal diffusivity (Section 1), and for the example shown, the ocean is bistable (ovals)

with the cold state being that emerged in Manabe and Stouffer (1988). One should note however, in contrast to the ocean-only model (Stommel 1961), it is the atmospheric coupling via the convective bound that allows this cold state of normal-signed differential density and MOC, which indeed is characterized by vanishing convective flux (Manabe and Stouffer 1988, their Fig. 18), as demanded by the convective bound.

For an eddying ocean, on the other hand, the admittance is not fixed by diapycnal diffusivity, but subjected to microscopic fluctuations associated with random eddy exchange across the subtropical front. Applying the fluctuation theorem (FT) --- a generalized second law (Crooks 1999), Ou (2018) deduces that the admittance would evolve over millennial timescale toward MEP, a process coined "MEP adjustment". It is seen therein that while MOC may contain a laminar component, so long as it is subjected to fluctuations, the MEP adjustment would be operative; varying the fluctuation amplitude only affects the adjustment timescale but not the MEP state. Although initial applications of MEP in climate theories involve guesswork (Paltridge 1975), subsequent developments have led to its growing acceptance (Ou 2001; Ozawa et al. 2003; Kleidon 2009), and if, as contended by Ou (2018), it were a deductive outcome of FT --- the latter being of considerable mathematical rigor and has been tested in laboratory (Evans and Searle 2002; Wang et al. 2002), it would further strengthen the physical basis of MEP. In addition, a recent direct numerical simulation (DNS) of horizonal convection has produced a mid-latitude front (Hogg and Gayen 2020), just as predicted by MEP (Ou 2006), to offer a tangible computational support. We recognize that MEP has not been applied in paleoclimate research, but hope that its demonstrated potency in accounting for glacial cycles would advance its future use.

To aid the visualization, we have blurred the MOC line in Fig. 2 to indicate microscopic fluctuations, whose probability bias in accordance with FT would pivot the MOC line over millennial timescale toward MEP, as marked by rectangles and discussed next.

1. Ocean bistates

As derived in Ou (2018), there is a MEP state in both warm and cold branches. The warm MEP is given by

$$(T^{'}, K) = (q^{'}, 1/2), \quad (2)$$

which will be referred as the interglacial (IG). The cold-box SST thus varies linearly with forcing, and as a cursory check, an absorbed SW flux 100 $W \bullet m^{-2}$ below the global mean, as representative of the current interglacial, would yield an averaged subpolar SST of 6 ^{0}C, not unlike that observed (Peixoto and Oort 1992, Fig. 8.8). Somewhat surprising, MOC is unaffected by forcing, which can be attributed to its shielding by the thermal response. In fact, from its scaling definition (Appendix B), we see that MOC is a function only of the air-sea transfer coefficient, a measurable and well-constrained quantity, and applying

its standard value yields a MOC of 14 Sv (for a basin width of 6000 km), which is commensurate with its observed strength (Macdonald 1998). Since the above deduction involves no free parameter, its observational test is more stringent than the ones involving tunned diapycnal diffusivity (Dalan et al. 2005).

The cold MEP is defined by freezing-point subpolar water

$T^{'} = T_f^{'}$ (3)

that is free of perennial ice, which we shall refer as the glacial (G). The coldness is consistent with the LGM observation that the polar front has migrated south to merge with the subtropical front (Ruddiman and McIntyre 1981, Fig. 26). And the deduced absence of perennial ice is because such ice would cut down the ocean cooling to weaken MOC, in contradiction to MEP. Since adjustment to MEP occurs over millennial timescale, this deduction does not preclude sea-ice formation over shorter timescales, including the seasonal one. In fact, with the subpolar water hovering around the freezing point, extensive sea ice necessarily forms in winter, as is the observed case (de Vernal et al. 2005), but tellingly the subpolar water remains largely open in summer (Sarnthein et al. 2003; de Vernal et al. 2005), in support of MEP. In addition to the freezing point, the subpolar water is significantly fresher and the MOC much weaker compared with the interglacial, both are consistent with LGM observations (de Vernal et al. 2005; Broecker and Denton 1989).

1. Hysteresis

For sub-millennial freshwater perturbations, the MOC line remains immobile, and it is readily seen from Fig. 2 that such perturbations, by moving the density curve up and down, may induce hysteresis between warm and cold branches, as seen in coupled models (Rahmstorf et al. 2005). Such short-term hysteresis however has no import on the orbital-induced hysteresis between MEP states propelled by pivoting MOC line, as illustrated in Fig. 3.

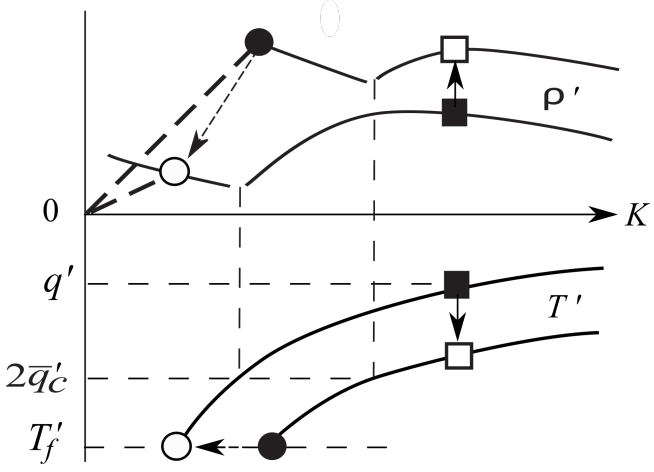

Figure 3: The evolution of the warm MEP (rectangles) when the absorbed SW flux $q^{'}$ is lowered (solid arrows) and the cold MEP (ovals) when $q^{'}$ is raised (dashed arrows). Thick dashed lines are the MOC lines associated with the cold MEP.

Suppose one is at the warm MEP (rectangles), a decreasing insolation would cool the water, as indicated by solid arrows, and when the temperature deficit exceeds the convective bound ($2\overline{q}_c^{'}$), the warm MEP no longer exists, and the ocean would enter the cold branch to propel toward the cold MEP. With (1) and (2), this cold transition $q_{\rm cold}^{'}$ occurs at

$$q_{\rm cold}^{'} = 2\overline{q}_c^{'}, \quad (4)$$

a function only of the global convective flux, an external parameter.

Now suppose one is at the cold MEP (ovals) of freezing point, then an increasing insolation would raise the temperature curve to propel the cold state, as indicated by dashed arrows, and flattening of the MOC line combined with fluctuations may vault the climate state into the warm branch, followed by its propelling toward the warm MEP. As a conservative upper bound of the warm transition $q_{\rm warm}^{'}$, it is set to when the MOC line is level to yield (Ou 2018, from his Eqs. 8 and 12)

$$q_{\rm warm}^{'} = (1+\mu)\overline{q}_c^{'} \ , \quad (5)$$

where μ is a "moisture-content" parameter derived from Clausius-Clapeyron equation with a standard value of 0.3 (Ou 2018).

The above two thresholds (4)-(5) define the "bistable interval", which thus is a function only of the global convective flux, and if this bistable interval is traversed by the orbital forcing, there would be hysteresis between the two MEP states.

3 Glacial cycles

To translate the possibility of ocean hysteresis to the particulars of glacial cycles, we need to first determine the relevant orbital forcing.

1. Orbital forcing

Having neglected its seasonal cycle, the ocean is heated by the annual absorbed SW flux. At orbital periods, this forcing is dominated by that over high latitudes, which is about an order of magnitude greater than that over the tropics (Berger et al. 2007, Fig. 2.7); and then over high latitudes, the forcing is dominated by that of the summer due both to the vanishing --- hence unvarying --- winter insolation (Berger 1988, Fig. 18b) and to the ice-albedo feedback that strongly amplifies the forcing range, as estimated later. These are general properties that do not distinguish obliquity and precession forcings, whose latitudinal difference (Short et al. 1991) is also partially allayed by spatial averaging over the subpolar water. This relative insensitivity to the forcing partition is consistent with model calculations of Calov and Ganopolski (2005).

On the other hand, we must recognize the critical importance of the ice-albedo feedback in instituting the precession forcing, which otherwise would be nil because of the Kepler's second law. This constraint is often overlooked and cannot be bypassed by ablation dependence on insolation (Huybers 2006) as the latter conflicts with its dominant control by the summer SAT (Pollard 1980). Since our forcing is the annual absorbed SW flux, the above Kepler stricture is naturally removed by activation of the ice-albedo feedback in late Pleistocene; and since glacial ice-albedo is known, its effect on the forcing can be readily quantified, as seen next.

Since the glacial state is characterized by an ice sheet extending to mid-latitudes, we take its ice albedo to be .3 (Peltier 1994, Fig. 4). Setting MI range of [450,550] $W \bullet m^{-2}$ (Berger et al. 1996, Fig. 3a) and subpolar attenuation of 20% by the atmospheric absorption and planetary albedo (Tricot and Berger 1988, Fig. 5), the summer absorbed SW flux has a range of $.8 \times (550 - 450 \times .7) = 188$ $W \bullet m^{-2}$, which would be halved to 94 $W \bullet m^{-2}$ for the annual mean. Although extremely crude, to the degree that it is of the same order as the MI range, we shall take MI as a convenient proxy for late Pleistocene forcing. We should stress that our use of MI is not because of its direct effect on the summer SAT, as widely applied previously (Abe-Ouchi et al. 2013; Huybers 2006), but because it mimics the annual absorbed SW flux that drives SST, which anchors the summer SAT.

3.2 Ice margin

To constrain the ice margin, we need to determine the latitudinal distribution of the summer SAT, which is assumed aligned with the SST because of the convective bound (Section 1). And to determine the subpolar SST distribution, we assume that it is at the freezing point at the Arctic rim because of the perennial Arctic sea-ice and that the ocean dynamics has smoothed its latitudinal gradient to render a linear profile, which thus is fully specified by the cold-box SST determined from the model. In accordance, the subpolar summer SAT is as sketched in Fig. 4: the thick sloping line for an interglacial and the x-axis for the glacial. The above deductions of the subpolar SST and summer SAT are broadly consistent with observations and model calculations (Peixoto and Oort 1992, Figs. 7.5 and 8.8; Ruddiman and McIntyre 1981, Fig. 26; Hostetler et al. 1999, Plate 1) hence adequate for our minimal model.

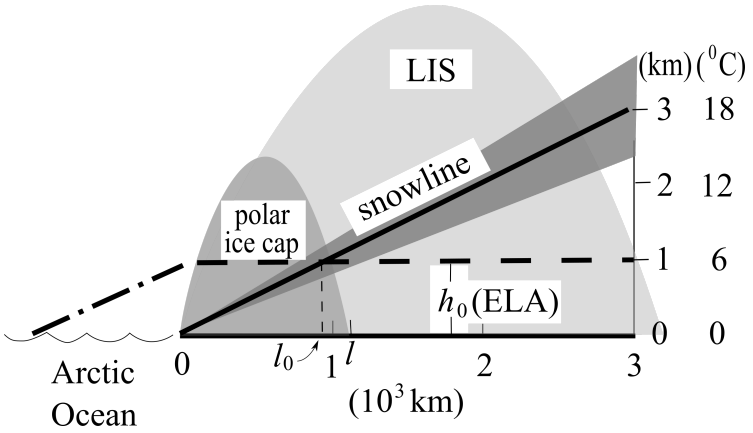

Figure 4: The summer SAT and snowline (the solid sloping line for interglacial and the x-axis for glacial), the shaded cone indicates perturbation by the orbital forcing. The ELA (dashed line) specifies the summer SAT of the ice margin (medium-shaded for interglacial and light-shaded for glacial). The dash-dotted line marks the snowline for transition to the ice-free state.

Assuming a constant lapse rate γ, the summer SAT line also represents the snowline (its height marked on the ordinate as well), whose intersect with the southern face of the ice sheet specifies the ELA (thick dashed). We shall next derive the ELA, which necessarily involves ice dynamics and mass balance, and again only the minimal balance is retained. For the ice dynamics, we assume a plastic ice sheet, so the momentum balance for the south-facing ice sheet states (Van der Veen 2013)

$d\left(h^2\right) = -c \bullet dx$ (6)

where h is the ice height and $c \equiv 2\tau_i \left(g\rho_i\right)^{-1}$ with τ_i, the yield stress, g, the gravitational acceleration and ρ_i, the ice density. We assume a melt rate of λT_i, where T_i is the ice surface temperature and , an empirical constant (Pollard 1980), and let l_0 and l be the x-coordinates of EL and ice margin, respectively, then the summer ablation is, invoking (6),

$$A_b = \int_{l_0}^{l} \lambda T_i \mathrm{dx}$$

$\approx \frac{}{c} \int_{h_0}^{0} \left(h_0 - h\right) d\left(h^2\right)$

$= \frac{}{3c} h_0^3$, (7)

a function only of the ELA. The accumulation A_c, being dominated by the summer snowfall above EL because of the much drier winter air, is roughly the summer moisture flux crossing the EL. Since this moisture flux is specified

by the energy flux and the moisture content (Ou 2007) --- both are strongly constrained by the EL being at the freezing point, the accumulation is largely insulated from the surface climate hence a robust property. Incidentally, with the accumulation dominated by the summer season when the ocean is ice-free --- even during LGM (Section 2.2), it discounts the sea-ice switch mechanism of the glacial cycles (Gildor and Tziperman 2000). Noting that we are concerned with the total accumulation above EL, which differs from local accumulation that can be strongly perturbed by surface climate (Alley et al. 1993). Equating the ablation and accumulation, we arrive at the ELA

$$h_0 \approx (\frac{3cA_c}{})^{1/3}. \quad (8)$$

Given the above constraint on the accumulation, it can be estimated from the summer moisture flux into the Arctic Ocean as the latter is rimmed by the freezing-point SAT, which is approximately $A_c = 2 \times 10^5 m^2/y$ (Peixoto and Oort 1992, Fig. 12.21). Setting additionally τ_i =1 bar (Weertman 1976), λ = 2 m (y ^{0}C) $^{-1}$ (Pollard 1980) and $\gamma = 6\ ^0$C km^{-1} (Weertman 1976), we estimate $h_0 = 1\ km$. Just as the accumulation is insensitive to the surface climate, so is the ELA, which thus is an inherent property of the ice sheet, and the above model-deduced estimate indeed agrees with that observed over the Greenland ice sheet (Oerlemans 1991). This ELA implies an ice margin aligned with the summer SAT of 6 ^{0}C (neglecting the SAT span over the narrow ablation zone), which incidentally may explain why the current Greenland is largely ice-covered since this isotherm lies along its southern edge (Peixoto and Oort 1992, Fig. 7.4b). Pegging the ice margin by a specific summer isotherm has been proposed by North et al. (1983), but their choice of 0 ^{0}C isotherm is deficient since there would be no summer ablation to counter the yearly accumulation, and then it would imply an ice-free Greenland, contradicting the observed one. Although there is uncertainty in the parameters of (8), the sensitivity is dampened by the 1/3 power, so this pegging of the ice margin by a summer SAT several degrees above the freezing point should generally apply, and a varying climate simply moves this isotherm (shaded in Fig. 4) hence the equilibrium ice margin.

From Fig. 4, we see that ocean bistates have translated into ice bistates of interglacial polar cap (medium-shaded) and glacial ice sheet extending to mid-latitudes (light-shaded). They differ fundamentally from that posited previously when the snowline, instead of pivoting by the varying climate, is displaced vertically (Weertman 1976; Oerlemans 1980), which results in bistates of an interglacial ice-free state and a varying glacial polar cap. Since the ice-free state requires a snowline intruding deep into the Arctic Ocean (dash-dotted), it implies a disappearance of the perennial ice, a condition unlikely to be realized since the northern hemisphere glaciation about 3 million years ago (Clark 1982). In our conception, on the other hand, it is the presence of the perennial Arctic ice that pins the snowline at the Arctic rim about which it pivots to render a variable polar cap: there is no ice-free state. And since the other bistate is an ice sheet extending to the mid-latitude aligned with the subtropical front, it can explain the southern extent of the Laurentide ice sheet (LIS) and why

all ice ages seem to have comparable ice volume (Carlson 2008, Fig. 2). This last observation arguably invalidates the previous conception of a glacial state characterized by variable polar ice cap --- in addition to the untenable ice-free state.

3.3 Pleistocene transitions

The MPT of glacial cycles from primarily obliquity to eccentricity periods poses a significant challenge to the astronomical theory since MI displays no discernible change. Besides the decreasing pCO_2 critiqued earlier (Section 1), the changing substrate geology has also been proposed (Clark et al. 2006), which however is poorly constrained by observations. The Pleistocene on the other hand exhibits pronounced cooling of O (10 ^{0}C), a continuing trend of the tertiary (Berger 1988, Fig. 4b) that is likely tectonic in origin because of the long timescale involved (Ruddiman and Raymo 1988). Addressing the tectonics obviously lies beyond the scope of this theory, which simply takes the Pleistocene cooling as an external factor and examines its effect on glacial cycles.

We have shown earlier that the bistable interval is defined by the global convective flux (Section 2.3), and we shall next argue that this flux is lowered during the Pleistocene cooling on account of the global-mean ocean heat balance, which states that the absorbed SW flux is countered by the net LW and convective fluxes. The absorbed SW flux would decrease by the expanding glaciation with its greater planetary albedo, and the net LW flux would increase due to drier air hence smaller downward LW flux; both thus reinforce each other to reduce the convective flux. As a crude estimate, an increase of the planetary albedo by 0.1 would reduce the absorbed SW flux by 30 $W \bullet m^{-2}$, and 10 ^{0}C cooling (Clark et al. 2006, Fig. 5a) would increase the net LW flux by also 30 $W \bullet m^{-2}$ (Previdi 2010, Fig. 1c), so together they would reduce the convective flux by 60 $W \bullet m^{-2}$, which is quite substantial considering it is currently of order 100 $W \bullet m^{-2}$ (Peixoto and Oort 1992, Fig. 6.3). Although there is no proxy data of the convective flux, the inferred large decrease underscores its robustness, which certainly dwarf the greenhouse effect of decreasing pCO_2 (several $W \bullet m^{-2}$, Mitchell et al. 1987), so does the observed cooling of O (10 ^{0}C) over the pCO_2-induced cooling of O (1 ^{0}C) (Broccoli and Manabe 1987; Petit et al. 1999). In all likelihood therefore, the direct effect of the drying air dominates that of the decreasing pCO_2 --- even though the latter is widely invoked to explain the MPT.

Based on the discussion to follow, we draw in Fig. 5 the time evolution of the forcing range (neglecting the obliquity and precession periods for illustration), which consists of three stages and their transitions. The three stages correspond to those depicted in Imbrie et al. (1993, Fig. 3) and their transitions, the early and middle Pleistocene transitions discerned by Lisiecki and Raymo (2007). The forcing range (cold-box deficit) is as marked on the ordinate and its centerline (thick-dashed) is referred as the mean forcing. The vertical bars are bistable intervals set by the global convective flux (4)-(5), which are moved upward by the Pleistocene cooling.

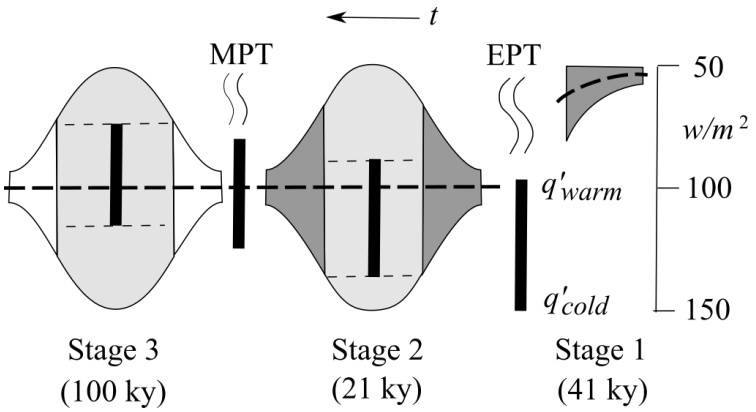

Figure 5: Evolution of the forcing envelope and ice signal (shaded) through Pleistocene, which consists of three stages and their transitions. The vertical bars are bistable intervals spanning cold ($q'_{\rm cold}$) and warm ($q'_{\rm warm}$) thresholds, which are moved up by Pleistocene cooling. Stage 1 is dominated by interglacial cycles (dark-shaded) at the 41-ky obliquity period; Stage 2 sees the emergence of G/IG cycles (light-shaded) at the 21-ky precession period; and Stage 3 is dominated by ice-age cycles (unshaded) at the 100-ky eccentricity period. Vertical bars drawn for Stage 2 and 3 correspond to global convective flux of 69 and 56 $W \bullet m^{-2}$ respectively.

At Stage 1 in the early Pleistocene, there is little ice-albedo feedback to effectuate the precession forcing (Section 3.1), so the ice signal is simply that of the polar ice cap varying linearly with obliquity. The forcing envelop is dark-shaded to symbolize the 41-ky interglacial cycles, which can be identified with the time span before 1.5 million years ago (Ma). The continuing cooling would enhance the ice-albedo feedback hence the precession forcing, both attaining maxima when the deepest precession trough $q'_{\rm max}$ exceeds the cold threshold (3) to generate the glacial state. This being the precondition of the full-fledged precession forcing that defines Stage 2, we thus set (from Eq. (3))

$$\overline{q}'_c = q'_{\rm max}/2 \quad (9)$$

as a crude marker for the early Pleistocene transition (EPT) from Stage 1 to 2, which can be identified with the time span of 1.5-1 Ma. Since the ice-albedo feedback primarily depresses the precession troughs (Section 3.1), the precession broadening of the forcing (hence ice-volume) envelop during EPT would manifest in the deepening of its mean, which indeed is a pronounced feature in observations (Lisiecki and Raymo 2005, Fig. 4).

Stage 2 is defined by full-fledged precession forcing (hence modulated by eccentricity) when the bistable centerline still lies below the mean forcing. Although glacial states are now generated by precession troughs during high eccentricity, they are invariably nullified by the next precession peaks, and the phase span

of this bistate oscillation is light-shaded to symbolize the presence of glacial ice sheet. Outside this phase span, the precession troughs no longer clear the cold threshold so there is only interglacial ice signal (hence dark-shaded). We identify Stage 2 with the time span of 1 to .7 Ma, which is characterized by emerging 21-ky G/IG cycles.

The continuing cooling elevates the bistable centerline to above the mean forcing, which defines Stage 3. There are again bistate oscillations during high eccentricity indicated by the light shade, outside of which however the precession peaks no longer clear the warm transition, so the glacial state would persist through low eccentricity to allow full growth of the ice sheet to mid-latitudes (hence unshaded). Stage 3 thus is dominated by the 100-ky ice-age cycles, which corresponds to the time span of .5 Ma to the present. The MPT from Stage 2 to 3 spans the time interval of .7-.5 Ma when the bistable centerline crosses the mean forcing, which can be seen from (3)-(4) to be given by

$\overline{q}_c^{'} = \frac{2}{3+\mu}\overline{q}^t$, (10)

where $\overline{q}^t$ is the mean forcing.

Although precession is not of zero period and transitions may span several hundred thousand years, the above deduction nonetheless provides testable criteria of Pleistocene transitions. For quantitative estimates, we set a mean forcing of 100 $W \bullet m^{-2}$ and forcing amplitude of 50 $W \bullet m^{-2}$ (Fig. 5), so EPT (9) and MPT (10) would be marked by global convective fluxes of 75 and 61 $W \bullet m^{-2}$, respectively. Since the global convective flux in early Pleistocene should be like the present interglacial hence of O (100 $W \bullet m^{-2}$) and the global convective flux is seen earlier to drop by several tens $W \bullet m^{-2}$ through Pleistocene, both deduced markers thus may be crossed to exhibit the observed transitions. The deduced power spectra of three stages should shift from that dominated by the obliquity to the emergence of the precession to that dominated by the eccentricity, as seen in the observed ones (Imbrie et al. 1993, Fig. 3).

For a coarser depiction, one may combine EPT, Stage 2 and MPT into a broader MPT corresponding to the traditional MPT from 41- to 100-ky cycles. Although its timing depends on the crossing of the deduced marker, its occurrence is inevitable given the Pleistocene cooling --- hence a robust feature of the model physics. In addition, we show that bistable G/IG states are sufficient to account for the varied glacial behavior: the ice ages are simply the glacial states lasting through low eccentricity that allow the ice sheet to grow to mid-latitudes (Ganopolski and Calov 2011), as attested by their common termination at the rising eccentricity (Raymo 1997; Lisiecki 2010). There is no need to invoke additional modes (Broecker and Denton 1989; Paillard 1998) whose physical basis is yet to be established.

3.4 Timeseries

To visualize the glacial cycles, we next present timeseries calculated for Stage 2 and 3 (there is no need to show Stage 1 characterized by interglacial signals

linear in the obliquity forcing). Since ice-albedo feedback hence the precession forcing is fully operative during these two stages, the model forcing can be approximated by MI (Section 3.1), which is set to

$q' = \overline{q}^t + \sum_{i=1}^{3} a_i cos\omega_i t.$ (11)

where the mean forcing is $\overline{q}^t$ =100 $W \bullet m^{-2}$, obliquity ($i = 1$) has a period of 41 ky and amplitude $a_1 = 10\ W \bullet m^{-2}$), and precessions ($i = 2$ and 3) have periods of 18.5 and 23 ky with amplitudes $a_2 = a_3 = 20\ W \bullet m^{-2}$, respectively, which renders a 21 ky precession modulated by 95 ky eccentricity, and a total forcing range of 100 $W \bullet m^{-2}$. Since MI is only a proxy for the actual forcing, above amplitudes are merely representative.

With the above forcing, our climate model would produce (time-varying) equilibrium cold-box SST (Section 2.2) and ice margin (Section 3.2), which are now subscripted "e" for distinction. To calculate the timeseries, we apply the relaxation equations:

$dT'/dt = (T'_e - T')/\tau_T$, (12)

and

$dl/dt = (l_e - l)/\tau_l$ (13)

where the time constant for temperature τ_T is the MEP adjustment time set at 1 ky and τ_l is the time constant for the ice margin, which we distinguish between ice advance and retreat. The ice advance is limited by accumulation: a snowfall of 0.3 m/y for example (Ohmura and Reeh 1991) would build up an ice sheet 3 km high in 10 ky, which is set to be the ice-advance time constant. The ice retreat can be much faster: for a 2 ^{0}C warming for example, the melt rate is 4 m/y (Pollard 1980), which is an order greater than the accumulation, we thus set the ice-retreat time constant to be 1 ky. The relaxation equations being linear, using different time constants merely affects the lag of the timeseries but produces no material difference.

We show in Fig. 6 timeseries and power spectra of the forcing (solid line), the cold-box SST (dashed) and ice margin (dotted) for Stage 2 and 3 with their global convective flux set to 69 and 56 $W \bullet m^{-2}$, respectively, as indicated by the drawn bistable intervals (the MATLAB script is provided in Appendix C). The initial condition is the warm MEP state and integration is carried forward for 400 ky; since the glacial cycles are largely repetitive, we plot only the last eccentricity cycle; the power spectra however are calculated for the full 400-ky timeseries. The upper axis represents the global-mean absorbed flux and SST. The forcing, being referenced to the former, is expressed in its temperature equivalent (100 $W \bullet m^{-2}$, for example, would convert to 8 ^{0}C, see Appendix B), the global-mean SST is set to 14 ^{0}C, the ice margin is its fractional extension into the subpolar, and the shaded horizonal bar marks the bistable interval.

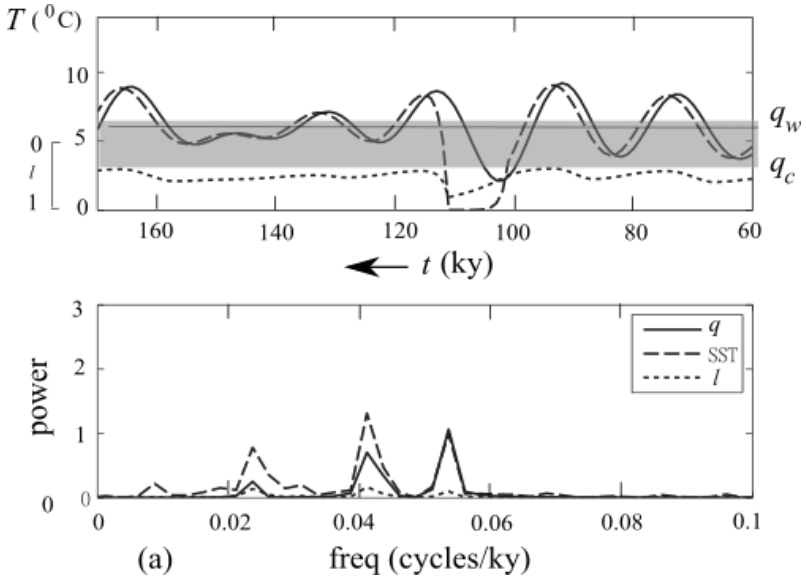

Figure 6(a): Timeseries and power spectra of the forcing (q, solid lines in equivalent temperature), subpolar SST (dashed, with a global-mean of 14 ^{0}C marking the upper axis) and ice margin (l, dotted, in fractional extension into the subpolar). The thin horizonal line is the mean forcing and the bistate interval (shaded bar) is that of Stage 2 shown in Fig. 5. There is only one episode of the glacial state lasting half precession period, so SST and ice-margin spectra exhibit only precession and obliquity peaks, just like the forcing.

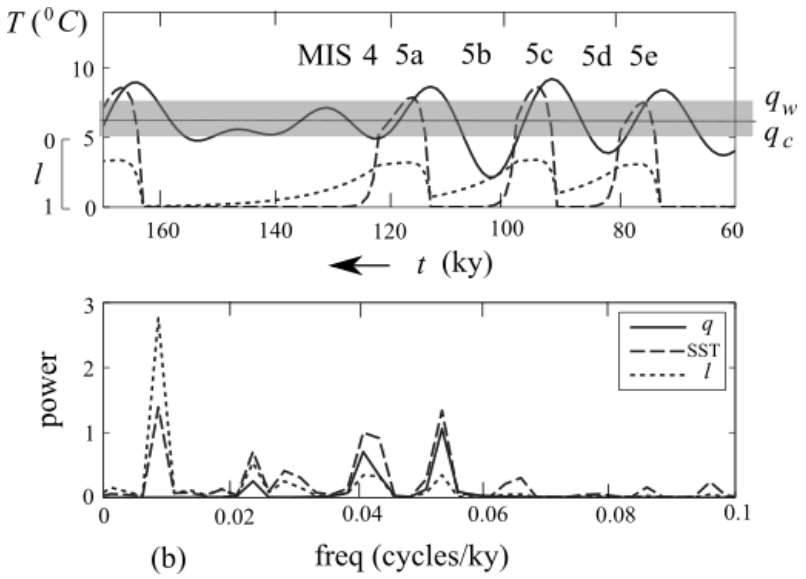

Figure 6(b): Same as Fig. 6a but for Stage 3 of Fig. 5 when the bistate interval (shaded bar) is further elevated by Pleistocene cooling. There are G/IG cycles during high eccentricity corresponding to the observed marine isotope stages, and a glacial state spanning the low eccentricity to allow full growth of the ice sheet to the mid-latitude. In contrast to Stage 2, the SST and ice-margin spectra exhibit strong eccentricity peaks absent in the forcing.

It is seen that the forcing timeseries resembles the observed Milankovitch insolation (Berger et al. 1996, Fig. 3a) and expectedly contains no power at the eccentricity period. The timeseries for Stage 2 (Fig. 6a) show that only one precession trough during high eccentricity has exceeded the cold threshold to generate the glacial state characterized by freezing-point SST and an ice sheet extending about half-way into the subpolar. Other than this single glacial episode lasting half the precession period, the rest of the timeseries are the interglacial SST that tracks the forcing with slight delay and small polar-cap variation. Given the short duration of the glacial state, the SST and ice-margin spectra show no appreciable power at the eccentricity period.

The timeseries of Stage 3 (Fig. 6b) differs qualitatively from that of Stage 2. There are episodes of interglacial during high precession peaks, which however always revert to glacial at the next precession trough and then there is only glacial spanning the low eccentricity, its long duration allows the ice sheet to grow to mid-latitudes. Although SST and ice-margin spectra retain the precession and obliquity peaks as Stage 2, they show a strong eccentricity peak that is absent in Stage 2. This sharp contrast is consistent with observations (Imbrie et al. 1993, Fig. 3).

The timeseries of Stage 3 bears sufficient resemblance to the last ice-age cycle

to allow labeling of the observed marine isotope stages (MIS), which thus may be interpreted by the model physics. According to our model, the cold substages are characterized by freezing-point subpolar water, which is consistent with observed expansion of the polar watermass and appearance of the polar species (McManus et al. 1994). Being a glacial state, the ice growth to the mid-latitude is only limited by the duration of the half precession period, which has nonetheless reached half-way to the subtropical front. This modelled ice sheet is consistent with observed sea-level change and ice-rafting events preconditioned on large ice sheet (Chapman and Shackleton 1999). In our interpretation, all substages are generically similar with the glacial at the cold substages reversed by the next precession peak to the interglacial warm substages, as seen in their comparable temperature (Keigwin et al. 1994). It is MIS 4 that heralds the onset of the ice age (Ruddiman et al. 1980) as the succeeding precession peak fails to clear the warm threshold, resulting in prolonged coldness and an ice sheet grown to mid-latitudes as manifested by LIS. It is noted that the ice margin is saw-toothed even within one precession trough due solely to the disparate its advance and retreat rates, and this asymmetry is strongly amplified for ice ages due to the ice growth through the low eccentricity before the rapid ice retreat.

1. **Resolving Pleistocene puzzles**

Our minimal model may resolve myriad Pleistocene puzzles, as highlighted below.

- 41-ky problem: Since the orbital forcing of the ocean is the annual absorbed SW flux, it would be affected by the ice-albedo feedback. In early Pleistocene before significant operation of this feedback, the precession forcing is nil because of the Kepler's second law. On the other hand, since the sea-level snowline hovers around the Arctic rim because of the perennial sea ice, there is always a finite polar ice cap (Fig. 4), thus exhibiting the 41-ky obliquity cycles.
- 100-ky problem: The enhanced ice-albedo feedback in late Pleistocene would remove the Kepler's stricture to institute the precession forcing. The bistates of an eddying ocean translate to disparate ice bistates to enable large ice-volume signal when the bistable interval is traversed by forcing. When the forcing fails to clear the warm threshold during decreasing eccentricity, the glacial would last through low eccentricity to allow the growth of LIS, resulting in 100-ky ice-age cycles paced by eccentricity.
- MPT problem: The bistable interval is set by the global convective flux, which is lowered during Pleistocene cooling on account of the surface heat balance. Combined with increasing ice-albedo feedback, it segregates the above accounts of 41- and 100-ky cycles to early and late Pleistocene, respectively, resulting in their mid-Pleistocene transition. Differing from previous conjectures, our theory provides a quantitative marker of the MPT, which can be tested against observation.
- 400-ky problem: So long as the ice-age pacing is enabled by eccentricity

of the shorter 100-ky period, the amplitude of the ice-age cycles is set by the intrinsic ice bistates hence unaffected by the longer-period 400 ky eccentricity even though it is of comparable amplitude (Imbrie et al. 1993, Fig. 2).

- Stage-11 problem: Despite intrinsic ice bistates, a smaller eccentricity nonetheless allows a longer-lasting ice age to augment the ice-volume signal, the 100-ky ice-age cycles thus may gain strength even when the eccentricity is decreasing (Clark et al. 1999, Fig. 6b) and it may explain why the lower eccentricity at Stage 11 is accompanied by stronger 100-ky cycles (Imbrie et al. 1993, Fig. 2).
- Variable termination problem: Since onset and termination of the ice age are threshold phenomena, both can be off by one precession period depending on precise timing, the ice-age cycles thus may vary between 80 and 120 ky (Raymo et al. 1997).
- Polar synchronization problem: Since Antarctica is iced over about 10 million years ago, there is no ice-albedo feedback to institute the precession forcing because of the Kepler's second law --- regardless its seasonal insolation is anti-phase with its northern counterpart (Clark et al. 1999). Then with glacial cycles dominated by the northern ice sheet, it would feedback into the global heat balance through ice albedo and atmospheric CO_2 (Broccoli and Manabe 1987) to synchronize the Antarctic climate, as suggested by its slight lag (Kawamura et al. 2007).

Various mechanisms have been proposed in solving these puzzles, our theory is notable in that it resolves them in a single dynamical framework and, differing from previous conjectures, our theory has produced specific markers of MPT that can be tested against observation.

1. **Discussion**

The central hypotheses of our theory are that the ocean is the intermediary of the orbital forcing of the ice sheet, and that the ocean is turbulent to be propelled toward MEP. To lessen the prospect of tunning, we aim for a minimal model to allow a more stringent test against observations. As such, simplifying assumptions are justified so long as they do not alter the basic closure to materially impact the model deductions.

One obvious question concerns the diapycnal diffusivity, typically regarded as essential in enabling MOC to overcome the potential-energy barrier (Colin de Verdière 1988). This conception however does not conflict with our MOC being specified by MEP hence independent of the diapycnal diffusivity (Section 2.2). This is because the potential-energy barrier depends also on the thermocline depth, which is no longer constrained by the laminar momentum balance, a degree of freedom that is in effect now closed by the MEP adjustment. Changing diapycnal diffusivity thus may be accommodated by varying thermocline depth without impacting the MOC.

Since MEP is a global property, it obviously negates the relevance of eddy diffusivity diagnosed from observation or derived from local turbulence closure, so to capture MEP adjustment from primitive-equation models, there is no substitute than resolving eddies, which obviously poses a significant challenge to glacial-cycle simulations because of the long integration needed. A phenomenological approach however may be feasible by implementing the MEP-adjustment equation of Ou (2018, Eq. 23) but replacing the admittance by the diapycnal diffusivity ν because of their power-law dependence. The equation now states

$$\frac{d(\ln \nu)}{\mathrm{dt}} = \left(\frac{\varepsilon}{n}\right)^2 \frac{d\ (\ln \sigma)}{d(\ln\ \nu)}\ , \quad (14)$$

where ε is the fluctuation amplitude set by the deformation radius, n, the exponent of the power law (about .5, Dalan et al. 2005) and σ, the entropy production, a product of the heat transport and differential temperature. Given a diapycnal diffusivity, one may calculate the entropy production from a coupled model, and from its neighboring points, one may calculate the right-hand side of the equation to allow its forward marching. This time-varying diapycnal diffusivity can be interpreted as its eddying-ocean equivalent, which thus should be greater than its measured value. This would produce a deeper thermocline via the mechanical energy balance, which is nonetheless consistent with the recognition that eddy exchanges expend little potential energy.

In our consideration of the glacial cycles, the ice sheet merely responds to the climate, but ice sheet is inherently unstable (Greve et al. 2006; Ou 2021), which may perturb the climate via meltwater fluxes. This climate/cryosphere coupling will be examined in a forthcoming paper on abrupt changes wherein we show that MEP adjustment may explain some their salient features as well to further support its utility. In conclusion, we have demonstrated through a minimal model that the mere posit of an eddying ocean as the intermediary of the orbital forcing of the ice sheet is sufficient to account for the observed glacial cycles and their transitions through the Pleistocene.

Appendix A: Acronyms

DNS Direct numerical simulation

EL Equilibrium line

ELA Equilibrium-line altitude

EPT Early Pleistocene transition

FT Fluctuation theorem

G/IG Glacial/interglacial

LGM Last glacial maximum

LIS Laurentide ice sheet

LW Long-wave

Ma Million years ago

MEP Maximum entropy production

MI Milankovitch insolation

MIS Marine isotope stage

MOC Meridional overturning circulation

MPT Mid-Pleistocene transition

NT Nonequilibrium thermodynamics

SAT Surface-air temperature

SST Sea-surface temperature

SW Short-wave

Appendix B: Symbols and standard values

A_b Ablation

A_c Accumulation ($= 2 \times 10^5 m^2/y$)

c Ice dynamics parameter ($= 2\tau_i \left(g\rho_i\right)^{-1}$)

$C_{p,o}$ Specific heat of ocean ($= 4.2 \times 10^3$J Kg $^{-1}K^{-1}$)

g Gravitational acceleration ($= 9.8\ m \bullet s^{-2}$)

h Ice-surface height

h_0 ELA

K Mass exchange rate of MOC

$[K]$ Scale of K ($= \alpha^* L(2\rho_o C_{p,o})^{-1} = 4.5 m^2/s$)

l x-coordinate of ice margin

l_e Equilibrium l

l_0 x-coordinate of ELA

L Latitudinal span of cold box ($= 3 \times 10^3$km)

q' Cold-box deficit of absorbed SW flux

$q'_{\max}$ Maximum q'

$\overline{q}^t$ Long-term mean of q' ($= 100\ W \bullet m^{-2}$)

$[q']$ scale of q' ($= \overline{q}^t = 100\ W \bullet m^{-2}$)

$\overline{q}'_c$ Global convective flux

a_i Amplitudes of Milankovitch insolation

$q_{\rm cold}^{'}$ Cold-transition threshold

$q_{\rm warm}^{'}$ Warm-transition threshold

S' Cold-box salinity deficit

$[S']$ Scale of $S'(=\alpha[T']/\beta$=1.79)

$\overline{T}$ Global-mean SST ($=14^0C$)

T' Cold-box SST deficit

$[T']$ Scale of $T'(=[q']/\ \alpha^*=8^0C)$

T_a' Cold-box SAT deficit (from global-mean SST)

T_e' Equilibrium T'

T_f' Freezing-point temperature

T_i Ice surface temperature

α Thermal expansion coefficient ($=1.7\times10^{-4}\bullet\ ^0C^{-1}$)

α^* Air-sea transfer coefficient ($=12.5\ W\bullet m^{-2}\bullet\ ^0C^{-1}$, Ou 2018)

β Saline contraction coefficient ($=7.6\times10^{-4}$)

γ Lapse rate ($=6^0C$/km)

ρ' Cold-box density surplus

$[\rho']$ Scale of ρ' ($=\rho_o\alpha[T']=1.36\ Kg\bullet m^{-3}$)

ρ_i Ice density ($=0.9\times10^3\ Kg\bullet m^{-3}$)

ρ_o Ocean density ($=10^3\ Kg\bullet m^{-3}$)

τ_i Yield stress ($=1\ bar$)

τ_l Ice-sheet time constant ($=1/10\ ky$ for retreat/advance)

τ_T MEP-adjustment time ($=1\ ky$)

λ Ice-melt parameter ($=2\ m\bullet y^{-1}\bullet\ ^0C^{-1}$)

μ Moisture-content parameter ($=0.3$)

ν Diapycnal diffusivity

Appendix C: MATLAB script for glacial cycles

% assign parameters

dt=1;tmax=400;t=(0:dt:tmax);m=length(t);m2=m/2;

fre1=2*pi/41;fre2=2*pi/18.5;fre3=2*pi/23;

amp1=0.8;amp2=1.6;amp3=1.6;

```
pha1=0;pha2=0;pha3=0;
dtemp1=4.5;qmean=8;dtemp2=2*dtemp1;
tempf=14;temp0=6;tausst=1;tauac=10;tauab=1;
gamma=0.3;
% set arrays
sste=zeros(1,m);sst=zeros(1,m);
icee=zeros(1,m);ice=zeros(1,m);
qprime=zeros(1,m);q=zeros(1,m);
% initialize with interglacial state (ig)
ig=true;
for i=1:(m-1)
%insolation
qprime(i)=amp1*cos(fre1*t(i)+pha1)...
+amp2*cos(fre2*t(i)+pha2)...
+amp3*cos(fre3*t(i)+pha3);
q(i)=qmean-qprime(i);
%calculate equilibrium temperature and ice margin
if ig
sste(i)=q(i);
temp1=tempf-sste(i);
icee(i)=0.5*temp0/temp1;
if q(i)>=dtemp2
ig=false;
end
end
if ~ig
sste(i)=tempf;
icee(i)=1;
if q(i)<=(1+gamma)*dtemp1
ig=true;
end
```

```
end
%time integration using runge-kutta scheme
sst(1)=sste(1);ice(1)=icee(1);
sst(i+1)=runge(sste(i),sst(i),dt,tausst);
ice(i+1)=rungeice(icee(i),ice(i),dt,tauac,tauab);
end
%rescale ice margin
ice5=5*(1-ice);
ice10=10*ice;
q=tempf-q;
sst=tempf-sst;
figure
% plot timeseries
subplot(2,1,1)
plot(t,q,'-k',t,sst,'--k',t,ice5,':k')
axis([60,170,0,tempf])
set(gca,'XDir','reverse');
%legend('q','sst','ice5','location','southeast')
title({['gla6a:','amp1=',num2str(amp1),',amp2=',num2str(amp2),...
',amp3=',num2str(amp3),',pha1=',num2str(pha1),...
',pha2=',num2str(pha2),',pha3=',num2str(pha3)];...
['dtemp1=',num2str(dtemp1),',qmean=',num2str(qmean),...
',temprange=',num2str(temprange),',tauac=',num2str(tauac),',tauab=',num2str(tauab),...
',gamma=',num2str(gamma)]})
xlabel('t (ky)');ylabel('temp')
% plot power spectra
yq=fft(qprime);
yq=fftshift(yq);
sstprime=sst-mean(sst);
ysst=fft(sstprime);
ysst=fftshift(ysst);
```

```
iceprime=ice10-mean(ice10);
yice=fft(iceprime);
yice=fftshift(yice);
f=(-m/2:m/2-1)/(dt*m);
powerq=2*abs(yq).^2/(m*m);
powersst=2*abs(ysst).^2/(m*m);
powerice=2*abs(yice).^2/(m*m);
subplot(2,1,2)
plot(f,powerq,'-k',f,powersst,'--k',f,powerice,':k')
axis([0,0.1,0,3])
legend('q','sst','ice')
xlabel('freq (cycles/ky)');ylabel('power')
% runge-kutta scheme for sst
function y=runge(x,r,dt,tau)
heating=@(r) (x-r)/tau;
k1 = heating(r);
k2 = heating(r+0.5*dt*k1);
k3 = heating(r+0.5*dt*k2);
k4 = heating(r+dt*k3);
y = r+1/6*dt*(k1+2*k2+2*k3+k4);
end
% runge-kutta scheme for ice margin
function y=rungeice(x,r,dt,tauac,tauab)
msign=x-r;
if msign<0
tau=tauab;
else
tau=tauac;
end
mbalance=@(r) (x-r)/tau;
k1 = mbalance(r);
```

k2 = mbalance(r+0.5*dt*k1);

k3 = mbalance(r+0.5*dt*k2);

k4 = mbalance(r+dt*k3);

y = r+1/6*dt*(k1+2*k2+2*k3+k4);

end

References

Abe-Ouchi A, Saito F, Kawamura K, Raymo ME, Okuno JI, Takahashi K, Blatter H (2013) Insolation-driven 100,000-year glacial cycles and hysteresis of ice-sheet volume. Nature 500(7461):190-193 https://doi.org/10.1038/nature12374

Adkins JF, Boyle EA, Keigwin L, Cortijo E (1997) Variability of the North Atlantic thermohaline circulation during the last interglacial period. Nature 390:154–156 https://doi.org/10.1038/36540

Alley RB, Meese DA, Shuman CA, Gow AJ, Taylor KC, Grootes PM, White JWC, Ram M, Waddington ED, Mayewski PA, Zielinski GA (1993) Abrupt increase in snow accumulation at the end of the Younger Dryas event. Nature 362:527-529 https://doi.org/10.1038/362527a0

Auer SJ (1987) Five-year climatological survey of the Gulf Stream system and its associated rings. J Geophys Res (92):11709–26 https://doi.org/10.1029/jc092ic11p11709

Berger A (1979) Spectrum of climatic variations and their causal mechanisms. Geophys Surveys 3(4), 351-402 https://doi.org/10.1007/bf01449756

Berger A (1988) Milankovitch theory and climate. Rev Geophys 26(4):624-57 https://doi.org/10.1029/rg026i004p00624

Berger A, Gallee H, Li XS, Dutrieux A, Loutre MF (1996) Ice sheet growth and high-latitudes sea surface temperature. Clim Dyn 12:441–448 https://doi.org/10.1007/s003820050119

Berger A, Li X, Loutre M (1999) Modeling northern hemisphere ice volume over the last 3 ma. Quat Sci Rev 18:1 – 11 https://doi.org/10.1016/s0277-3791(98)00033-x

Berger A, Loutre MF, Kaspar F, Lorenz SJ (2007) Chapter 2. Insolation during interglacial. In Developments in Quaternary Sciences (Vol. 7, 13-27), Elsevier https://doi.org/10.1016/s1571-0866(07)80027-3

Broccoli AJ, Manabe S (1987) The influence of continental ice, atmospheric CO_2, and land albedo on the climate of the last glacial maximum. Clim Dyn 1(2):87-99 https://doi.org/10.1007/bf01054478

Broecker WS, Denton GH (1989) The role of ocean-atmosphere reorganization in glacial cycles. Geochim Cosmochim Acta 53:2465-501 https://doi.org/10.1016/0016-7037(89)90123-3

Calov R, Ganopolski A (2005) Multistability and hysteresis in the climate-cryosphere system under orbital forcing. Geophys Res Lett 32:L21717 https://doi.org/10.1029/2005gl024518

Carlson A (2008) Why there was not a Younger Dryas-like event during the Penultimate Deglaciation? Quat Sci Rev 27(9–10):882–7 https://doi.org/10.1016/j.quascirev.2008.02.004

Chapman MR and Shackleton NJ (1999) Global ice-volume fluctuations, North Atlantic ice-rafting events, and deep-ocean circulation changes between 130 and 70 ka. Geology 27, 795–8 https://doi.org/10.1130/0091-7613(1999)027<0795:givfna>2.3.co;2

Clark DL (1982) Origin, nature and world climate effect of Arctic Ocean ice-cover. Nature 300(5890):321-5 https://doi.org/10.1038/300321a0

Clark PU, Alley RB, Pollard D (1999) Northern Hemisphere ice sheet influences on global climate change. Science 286:1104–11 https://doi.org/10.1126/science.286.5442.1104

Clark PU, Archer D, Pollard D, Blum JD, Rial JA, Brovkin V, Mix AC, Pisias NG, Roy M (2006) The middle Pleistocene transition: characteristics, mechanisms, and implications for long-term changes in atmospheric pCO2. Quat Sci Rev 25:3150-84 https://doi.org/10.1016/j.quascirev.2006.07.008

CLIMAP PM (1976) The surface of the ice-age earth. Science 191(4232):1131-7 https://doi.org/10.1126/science.191.4232.1131

Colin de Verdière A (1988) Buoyancy driven planetary flows. J Mar Res 46:215–65 https://doi.org/10.1357/002224088785113667

Crooks GE (1999) Entropy production fluctuation theorem and the nonequilibrium work relation for free energy differences. Phys Rev E 60(3):2721-6 https://doi.org/10.1103/physreve.60.2721

Crucifix M (2013) Why could ice ages be unpredictable? Clim Past (9):2253-67 https://doi.org/10.5194/cp-9-2253-2013

Dalan F, Stone P, Kamenkovich IV, Scott JR (2005) Sensitivity of the Ocean's Climate to Diapycnal Diffusivity in an EMIC. Part I: Equilibrium State. J Clim 18:2460-81 https://doi.org/10.1175/jcli3411.1

Dansgaard W, Johnsen S, Clausen HB, Dahl-Jensen D, Gundestrup N, Hammer CU, Hvldberg CS, Steffensen JP, Sveinbjornsdottir AE, Jouzel J, Bond G (1993) Evidence for general instability of past climate from a 250-kyr ice-core record. Nature 364:218–20 https://doi.org/10.1038/364218a0

de Vernal A, Eynaud F, Henry M, Hillaire-Marcel C, Londeix L, Mangin S, Matthiessen J, Marret F, Radi T, Rochon A, Solignac S, Turon JL (2005) Reconstruction of sea surface conditions at middle to high latitudes of the Northern Hemisphere during the Last Glacial Maximum (LGM) based on dinoflagellate cyst assemblages. Quat Sci Rev (24):897–924 https://doi.org/10.1016/j.quascirev.2004.06.014

Elkibbi M, Rial JA (2001) An outsider's review of the astronomical theory of the climate: is the eccentricity-driven insolation the main driver of the ice ages? Earth Sci Rev 56(1-4):161-77 https://doi.org/10.1016/s0012-8252(01)00061-7

Evans DJ, Searle DJ (2002) The fluctuation theorem. Adv Phys 51:1529 https://doi.org/10.1080/00018730210155133

Ganopolski A, Brovkin V (2017) Simulation of climate, ice sheets and CO2 evolution during the last four glacial cycles with an Earth system model of intermediate complexity. Clim Past 13:1695–716 https://doi.org/10.5194/cp-13-1695-2017

Ganopolski A, Calov R (2011) The role of orbital forcing, carbon dioxide and regolith in 100 kyr glacial cycles. Clim Past 7:1415-25 https://doi.org/10.5194/cp-7-1415-2011

Ghil M (1994) Cryothermodynamics: The chaotic dynamics of paleoclimate. Physica D 77:130–59 https://doi.org/10.1016/0167-2789(94)90131-7

Gildor H, Tziperman E (2000) Sea ice as the glacial cycles climate switch: Role of seasonal and orbital forcing. Paleoceanogr 15:605-15 https://doi.org/10.1029/1999pa000461

Greve R, Takahama R, Calov R (2006) Simulation of large-scale ice-sheet surges: the ISMIP HEINO experiments. Polar Meteor Glaciol 20:1-5

Hays JD, Imbrie J, Shackleton NJ (1976) Variations in the Earth's orbit: pacemaker of the ice ages. Science 194(4270):1121-32 https://doi.org/10.1126/science.194.4270.1121

Hogg AM, Gayen B (2020) Ocean gyres driven by surface buoyancy forcing. Geophys Res Lett 47:e2020GL088539 https://doi.org/10.1029/2020GL088539

Honisch B, Hemming NG, Archer D, Siddall M, McManus JF (2009) Atmospheric carbon dioxide concentration across the mid-Pleistocene transition. Science 324:1551-4 https://doi.org/10.1126/science.1171477

Hostetler SW, Clark PU, Bartlein PJ, Mix AC, Pisias NJ (1999) Atmospheric transmission of north Atlantic Heinrich events. J Geophys Res Atm 104(D4):3947-52 https://doi.org/10.1029/1998jd200067

Huybers P (2006) Early Pleistocene glacial cycles and the integrated summer insolation forcing. Science 313(5786):508-11 https://doi.org/10.1126/science.1125249

Imbrie J, Berger A, Boyle E, Clemens SC, Duffy A, Howard WR, Kukla G, Kutzbach J, Martinson DG, McIntyre A, Mix AC, Molfino B, Morley JJ, Peterson LC, Pisias NG, Prell WL, Raymo ME, Shackleton NY, Toggweiler JR (1993) On the structure and origin of major glaciation cycles 2. The 100,000-year cycle. Paleoceanogr 8(6):699-735 https://doi.org/10.1029/93pa02751

Imbrie J, Imbrie JZ (1980) Modeling the Climatic Response to Orbital Variations. Science 207:943-53 https://doi.org/10.1126/science.207.4434.943

Imbrie JZ, Imbrie-Moore A, Lisiecki LE (2011) A phase-space model for Pleistocene ice volume. Earth Planet Sci Lett 307(1-2):94-102 https://doi.org/10.1016/j.epsl.2011.04.018

Kawamura K, Parrenin F, Lisiecki L, Uemura R, Vimeux F, Severinghaus JP, Hutterli MA, Nakazawa T, Aoki S, Jouzel J, Raymo ME (2007) Northern Hemisphere forcing of climatic cycles in Antarctica over the past 360,000 years. Nature 448(7156):912-6 https://doi.org/10.1038/nature06015

Keigwin LD, Curry WB, Lehman SJ, Johnsen S (1994) The role of the deep ocean in North Atlantic climate change between 70 and 130 kyr ago. Nature 371(6495):323-6 https://doi.org/10.1038/371323a0

Kleidon A (2009) Non-equilibrium thermodynamics and maximum entropy production in the Earth system: applications and implications. Naturwiss 96:653–77 https://doi.org/10.1007/s00114-009-0509-x

Labeyrie L, Vidal L, Cortijo E, Paterne M, Arnold M, Duplessy JC, Vautravers M, Labracherie M, Dupart J, Turon JL, Grousset F, van Weering T (1995) Surface and deep hydrology of the Northern Atlantic Ocean during the last 150000 years. Phil Trans R Soc Lon 348:255-64 https://doi.org/10.1098/rstb.1995.0067

Lisiecki LE (2010) Links between eccentricity forcing and the 100,000-year glacial cycle. Nature Geos 3:349-52 https://doi.org/10.1038/ngeo828

Lisiecki LE, Raymo MEA (2005) Pliocene-Pleistocene stack of 57 globally distributed benthis δ^{18}O records. Paleoceanogr 20:PA1003 https://doi.org/10.1029/2004PA001071

Lisiecki LE, Raymo ME (2007) Plio–Pleistocene climate evolution: trends and transitions in glacial cycle dynamics. Quat Sci Rev 26(1):56-69 https://doi.org/10.1016/j.quascirev.2006.09.005

Lozier MS (2010) Deconstructing the conveyer belt. Science 328(5985):1507-11 http://doi.org/10.1126/science.1189250

Macdonald A M (1998) The global ocean circulation: A hydrographic estimate and regional analysis. Progr Oceanogr 41(3):281-382 https://doi.org/10.1016/s0079-6611(98)00020-2

Manabe S, Stouffer RJ (1988) Two stable equilibria of a coupled ocean-atmosphere model. J Clim 1:841-66 https://doi.org/10.1175/1520-0442(1988)001<0841:tseoac>2.0.co;2

Marotzke J, Stone P (1995) Atmospheric transports, the thermohaline circulation, and flux adjustments in a simple coupled model. J Phys Oceanogr 25:1350-64 https://doi.org/10.1038/287430a0

McManus JF, Bond GC, Broecker WS, Johnsen S, Labeyrie L, Higgins S (1994) High-resolution climate records from the N. Atlantic during the last interglacial. Nature 371:326–9 https://doi.org/10.1038/371326a0

Milankovitch M (1941) Canon of insolation and the ice-age problem. R Serb Acad Spec Publ 132 (Translated from German, Israel Program for Scientific Translations) Jerusalem, 1969

Mitchell JFB, Wilson CA, Cunnington WM (1987) On CO2 climate sensitivity and model dependence of results. Q J R Meteorolog Soc 113:293–322 https://doi.org/10.1002/qj.49711347517

North GR, Mengel JG, Short DA (1983) Simple energy balance model resolving the seasons and the continents: Application to the astronomical theory of the ice ages. J Geophys Res 88(C11):6576-86 https://doi.org/10.1029/jc088ic11p06576

Oerlemans J (1980) Model experiments on the 100,000-yr glacial cycle. Nature 287(5781):430-2 https://doi.org/10.1038/287430a0

Oerlemans J (1982) Glacial cycles and ice-sheet modelling. Clim Change 4(4):353-74 https://doi.org/10.1007/bf02423468

Oerlemans J (1991) The mass balance of the Greenland ice sheet: sensitivity to climate change as revealed by energy-balance modelling. Holocene 1(1):40-8 https://doi.org/10.1177/095968369100100106

Ohmura A, Reeh N (1991) New precipitation and accumulation maps for Greenland. J Glaciol 37(125):140-8 https://doi.org/10.3189/s0022143000042891

Ou HW (2001) Possible bounds on the earth's surface temperature: From the perspective of a conceptual global-mean model. J Clim 14:2976-88 https://doi.org/10.1175/1520-0442(2001)014<2976:pbotes>2.0.co;2

Ou HW (2006) Meridional thermal field of a coupled ocean-atmosphere system: a conceptual model. Tellus 58A:404-15 https://doi.org/10.1111/j.1600-0870.2006.00174.x

Ou HW (2007) Hydrological cycle and ocean stratification in a coupled climate system: a theoretical study. Tellus 59A:683-94 https://doi.org/10.3402/tellusa.v59i5.15157

Ou HW (2018) Thermohaline circulation: a missing equation and its climate change implications. Clim Dyn 50:641–53 https://doi.org/10.1007/s00382-017-3632-y

Ou HW (2021) A theory of glacier dynamics and instabilities Part 1: Topographically confined glaciers. J Glaciol:1–12 https://doi.org/10.1017/jog.2021.20

Ozawa H, Ohmura A, Lorenz RD, Pujol T (2003) The second law of thermodynamics and the global climate system: A review of the maximum entropy production principle. Rev Geophys 41:4/10182003 https://doi.org/10.1029/2002rg000113

Paillard D (1998) The timing of Pleistocene glaciations from a simple multiple-state climate model. Nature 391:378-81 https://doi.org/10.1038/34891

Paltridge GW (1975) Global dynamics and climate—-A system of minimum entropy exchange, Q J R Meteorol Soc 101:475–484 https://doi.org/10.1002/qj.49710142906

Peixoto JP, Oort AH (1992) Physics of Climate. Amer Inst Phys, New York https://doi.org/10.1063/1.2809772

Pelletier JD (2003) Coherence resonance and ice ages. J Geophys Res 108(D20):4645 https://doi.org/10.1029/2002jd003120

Peltier WR (1994) Ice age paleotopography. Science 265:195–201 https://doi.org/10.1126/science.265.5169.195

Petit JR, Jouzel J, Raynaud D, Barkov NI, Barnola JM, Basile I, Bender M, Chappellaz J, Davis M, Delaygue G, Delmotte M (1999) Climate and atmospheric history of the past 420,000 years from the Vostok ice core, Antarctica. Nature 399(6735):429-36 https://doi.org/10.1038/20859

Pollard D (1980) A simple parameterization for ice sheet ablation rate. Tellus 32(4):384-8 https://doi.org/10.1111/j.2153-3490.1980.tb00965.x

Pollard D (1983) A coupled climate-ice sheet model applied to the Quaternary ice ages. J Geophys Res 88(C12):7705-18 https://doi.org/10.1029/jc088ic12p07705

Previdi M (2010) Radiative feedbacks on global precipitation. Environ Res Lett 5(2):025211 https://doi.org/10.1088/1748-9326/5/2/025211

Rahmstorf S, Crucifix M, Ganopolski A, Goosse M, Kamenkovich I, Knutti R, Lohmann G, Marsh R, Mysak LA, Wang Z, Weaver AJ (2005) Thermohaline circulation hysteresis: A model intercomparison. Geophys Res Lett 32(23) L23605 https://doi.org/10.1029/2005gl023655

Ravelo AN, Andreasen DH, Lyle M, Lyle AO, Wara MW (2004) Regional climate shifts caused by gradual global cooling in the Pliocene epoch. Nature 429:263-7 https://doi.org/10.1038/nature02567

Raymo ME (1997) The timing of major climate terminations. Paleoceanogr 12(4):577-85 https://doi.org/10.1029/97pa01169

Raymo ME, Nisancioglu KH (2003) The 41 kyr world: Milankovitch's other unsolved mystery. Paleoceanogr 18(1) https://doi.org/10.1029/2002pa000791

Raymo ME, Oppo DW, Curry W (1997) The mid-Pleistocene climate transition: a deep sea carbon isotopic perspective. Paleoceanogr 12(4):546-59 https://doi.org/10.1029/97pa01019

Ruddiman WF, McIntyre A (1981) The North Atlantic Ocean during the last deglaciation. Palaeogeogr Palaeoclimatol Palaeoecol 35:145-214 https://doi.org/10.1016/0031-0182(81)90097-3

Ruddiman WF, McIntyre A, Niebler-Hunt V, Durazzi JT (1980) Oceanic evidence for the mechanism of rapid northern hemisphere glaciation. Quat Res 13(1):33-64 https://doi.org/10.1016/0033-5894(80)90081-2

Ruddiman W, Raymo M (1988) Northern Hemisphere climate regimes during the past 3 Ma: Possible tectonic connections. Phil Trans R Soc London Ser B 318:411-30 https://doi.org/10.1098/rstb.1988.0017

Saltzman B, Hansen A, Maasch K (1984) The late Quaternary glaciations as the response of a three-component feedback system to Earth-

orbital forcing. J Atmos Sci 41:3380–9 https://doi.org/10.1175/1520-0469(1984)041<3380:tlqgat>2.0.co;2

Sarnthein M, Pflaumann U, Weinelt M (2003) Past extent of sea ice in the northern North Atlantic inferred from foraminiferal paleotemperature estimates. Paleoceanogr 18(2) https://doi.org/10.1029/2002pa000771

Shackleton N (2000) The 100,000-year ice-age cycle identified and found to lag temperature, carbon dioxide, and orbital eccentricity. Science 289:1897– 902

Short DA, Mengel JG, Crowley TJ, Hyde WT, North GR (1991) Filtering of Milankovitch cycles by Earth's geography. Quat Res 35(2):157-73 https://doi.org/10.1016/0033-5894(91)90064-c

Siegenthaler U, Stocker TF, Monnin E, Lüthi D, Schwander J, Stauffer B, Raynaud D, Barnola JM, Fischer H, Masson-Delmotte V, Jouzel J (2005) Stable carbon cycle–climate relationship during the late Pleistocene. Science 310(5752):1313-7 https://doi.org/10.1126/science.1120130

Stommel H (1961) Thermohaline convection with two stable regimes of flow. Tellus 13:224-30 https://doi.org/10.1111/j.2153-3490.1961.tb00079.x

Suarez MJ, Held IM (1979) The sensitivity of an energy balance climate model to variations in the orbital parameters. J Geophys Res Oceans 84(C8):4825-36 https://doi.org/10.1029/jc084ic08p04825

Tricot C, Berger A (1988) Sensitivity of present-day climate to astronomical forcing. In *Long and Short Term Variability of Climate* (p. 132-52), Springer Berlin Heidelberg https://doi.org/10.1007/bfb0046593

Tziperman E, Raymo ME, Huybers PJ, Wunsch C (2006) Consequences of pacing the Pleistocene 100 kyr ice ages by nonlinear phase locking to Milankovitch forcing. Paleoceanogr 21(PA4206):1-11 https://doi.org/10.1029/2005pa001241

Van der Veen CI (2013) Fundamentals of glacier dynamics, CRC Press (second edition), Boca Raton, FL, 403 pp. https://doi.org/10.1201/b14059

Wang GM, Sevick EM, Mittag E, Searles DJ, Evans DJ (2002) Experimental demonstration of violations of the Second Law of Thermodynamics for small systems and short time scales. Phys Rev Lett 89 (5):050601/1–050601/4 https://doi.org/10.1103/physrevlett.89.050601

Weertman J (1976) Milankovitch solar radiation variations and ice age ice sheet sizes. Nature 261:17-20 https://doi.org/10.1038/261017a0

Wunsch C (2003) The spectral description of climate change including the 100 ky energy. Clim Dyn 20(4):353-63 https://doi.org/10.1007/s00382-002-0279-z